JOURNAL OF GEOPHYSICAL RESEARCH, VOL. 99, NO. C7, PAGES 14,159–14,171, JULY 15, 1994

Diagnostic and prognostic calculations of the North Atlantic circulation and sea level using a sigma coordinate ocean model

Tal Ezer and George L. Mellor

Program in Atmospheric and Oceanic Sciences, Princeton University, Princeton, New Jersey

Abstract. The North Atlantic circulation and sea surface height, determined from hydrographic and wind stress data are calculated with a free surface, primitive equation ocean model. The model grid, a vertical sigma - coordinate and horizontal curvilinear orthogonal system, makes it possible to resolve coastal regions with complicated topography that were unresolved in previous calculations. When running in a diagnostic mode, in which the temperature and the salinity fields are fixed and equal to the Levitus annual mean fields, the vertically integrated North Atlantic circulation is very similar to though more detailed than that obtained from previous calculations using simpler diagnostic models. On the other hand, the meridional, zonally averaged flows and the poleward heat transport from the purely diagnostic calculations are noisy and unrealistic. However, short prognostic calculations of only 30 days following the diagnostic run allow intensification of the western boundary current and removal of noise due to inconsistencies between the hydrographic data and bottom topography and produce a more realistic meridional circulation and poleward heat transport, with a maximum value of 1.2×10^{15} W which is, comparable to estimates based on observations. The calculated sea level along the North America continent agrees with previous estimates but provides more spatial detail. Analysis of the dynamic adjustment process shows that this process is dominated by the effect of bottom topography through the action of the bottom pressure torque. This study is a first step in applying a realistic numerical model, previously used primarily for estuaries and coastal regions, to basin-scale ocean problems.

1. Introduction

For many years, oceanographers sought to determine the thermohaline and wind-driven circulation of the ocean from observed hydrographic and wind stress measurements. A recent study by *Marotzke and Wunsch* [1993], however, questions the existence of such a state which is consistent with the observed hydrography and forcing. Calculations of this type, which neglect time-dependent processes and assume a steady state solution, are sometimes called diagnostic calculations. The different approaches for such calculations range from a simple geostrophic calculation to more complicated models. To calculate the North Atlantic circulation, *Holland and Hirschman* [1972] used a primitive equation model integrated to steady state. *Sarmiento and Bryan* [1982] used a robust diagnostic model based on a numerical dynamic model together with a Newtonian damping term which constrains the model fields back to the observed climatology. This methodology has also been used recently by *Fujio et al.* [1992] for global ocean circulation studies and by *Saunders and Thompson* [1993] for diagnostic calculations of the Southern Ocean. Another approach to estimating the ocean state due to forcing constraints is the optimization technique using inverse methods [*Wunsch*, 1978; *Tziperman et al.*, 1992; *Marotzke and Wunsch*, 1993]. However, the latter technique is computationally quite expensive and thus often requires the use of simplified models with coarse resolution. A simpler method is the diagnostic model applied by *Kantha et al.* [1982] to the circulation of the South Atlantic Bight, by *Mellor et al.* [1982] to the Atlantic Ocean, and by *Greatbatch et al.* [1991] to climatic changes in the North Atlantic circulation due to changes in observed thermal structure and winds. The model calculates the circulation from hydrography and wind stress (τ) data by integrating the vorticity balance equation

$$\mathbf{J}(\Psi, f/H) = \mathbf{J}(\Phi, 1/H) + 1/\rho_0 \mathrm{curl}(\tau/H) \quad (1)$$

along potential vorticity (f/H) contours (f is the Coriolis parameter; $H(\lambda,\phi)$ is bottom topography). Here Ψ is the total stream function; Φ is the potential energy per unit area of the water column; $J(A,B) \equiv \cos^{-1}(\phi)R^{-2}[(\partial A/\partial\phi)(\partial B/\partial\lambda) - (\partial A/\partial\lambda)(\partial B/\partial\phi)]$ is the Jacobian operator; and λ, ϕ, ρ_0 and R are the longitude, latitude, reference density, and Earth radius, respectively. The first term on the right-hand side of (1) is the joint effect of baroclinicity and bottom relief (the so-called JEBAR effect [*Sarkisyan and Ivanov*, 1971; *Holland*, 1973]. The JEBAR term can be separated into two parts; one is associated with the bottom pressure torque (discussed later) corresponding to the interaction of bottom pressure and bottom topography, and the second is associated with the compensation by the density stratification for the effect of variable bottom topography (see *Greatbatch et al.* [1991] for more detail).

Figure 1 shows the North Atlantic circulation as calculated by *Mellor et al.* [1982] using an early release of the *Levitus* [1982] hydrographic data and the *Hellerman and Rosenstein*

Paper number 94JC00859.
0148-0227/94/94JC-00859$05.00

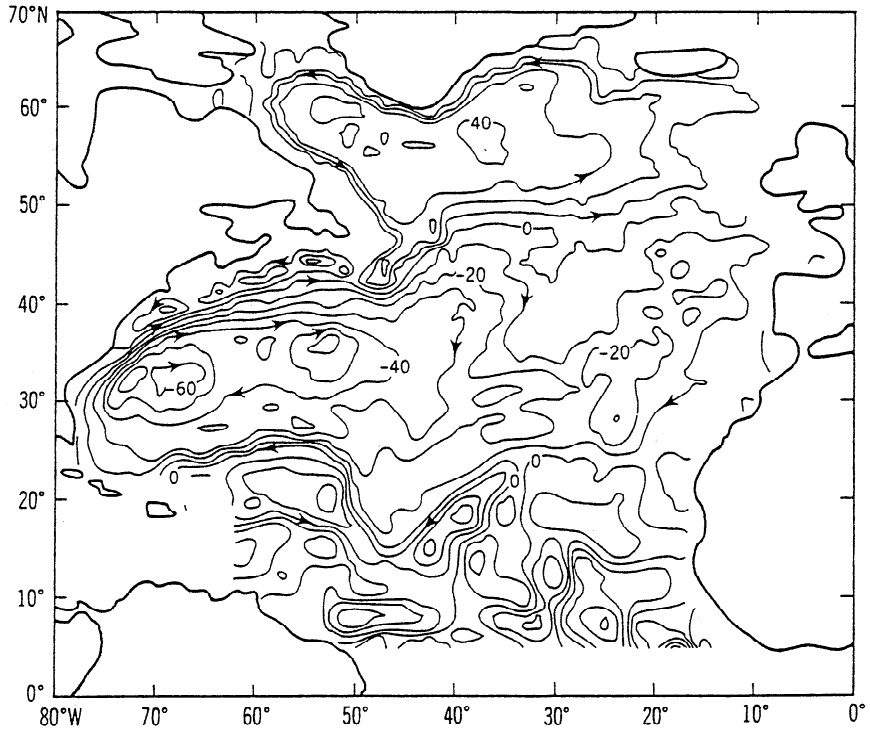

Figure 1. The vertically integrated horizontal transport of the North Atlantic calculated from a diagnostic model [Mellor et al., 1982] using (1). The contour interval of the total stream function is 10 Sv.

[1983] wind stress data. Although this diagnostic model is quite simple and is based on a coarse resolution (1^{O} x 1^{O}) data, it nevertheless produced a fairly detailed description of the circulation and compares well with observations. For example, the Gulf Stream transport is about 90 Sv (1 Sv = 10^6 m^3 s^{-1}), and about 25 Sv of this transport derived from a southwestward current that flows along the continental slope and is entrained into the Gulf Stream. The existence of the latter feature, known now as the northern recirculation gyre, has been confirmed by observations [e.g., *Richardson*, 1985; *Hogg et al.*, 1986] but was missing from some other diagnostic models [*Holland and Hirschman*, 1972; *Sarmiento and Bryan*, 1982]. This recirculation gyre plays an important role in the separation of the Gulf Stream from the coast, as indicated by the study by *Ezer and Mellor* [1992]. Limitations of the *Mellor et al.* [1982] model are that for equatorial regions, where f is small, and regions with complicated topography (e.g., the Caribbean Sea) calculations could not be done. We will evaluate the diagnostic model presented above, based on (1), by comparing it to the solution based on the full three-dimensional, primitive equation model.

The approach taken here is to apply a primitive equation model, the Princeton ocean model [*Blumberg and Mellor*, 1987; *Mellor*, 1992], to make a diagnostic calculation (temperature and salinity held constant) followed by a short-term prognostic calculation to adjust the observed density field to the topography and surface forcing by using the model dynamics. A similar approach has been suggested before [*Demin et al.*, 1990], and the timescale for such an adjustment was shown to be relatively short compared with seasonal and advective time scales, (about 30-40 days in equatorial regions and only 5-7 days in middle latitudes) based on the time-dependent behavior of kinetic energy and enstrophy.

Using a primitive equation, free surface ocean model for diagnostic calculations yields dynamically adjusted (nearly geostrophic) velocities and surface elevations. *Mellor and Ezer* [1991] and *Ezer and Mellor* [1992] used this type of diagnostic calculations together with climatological data to initialize a regional western North Atlantic model and to study altimetric data assimilation techniques and Gulf Stream separation. Diagnostic calculations with synoptic data (representing satellite observations taken around a specific day) have also been used by *Ezer et al.* [1992, 1993] for initialization of nowcast and forecast experiments. This, however, is the first attempt to implement a realistic model of this type (i.e., with a second-order turbulence scheme, free surface, and coastal topography) for the entire North Atlantic basin. Other basin-scale and global eddy-resolving models [e.g., *Bryan and Holland*, 1989; *Treguier*, 1992; *Semtner and Chervin*, 1992; *Oberhuber*, 1993] do not at this time resolve the continental shelf and slope regions and may have difficulties simulating realistic Gulf Stream separation. Meridional circulation and heat transport in ocean models may also have some deficiencies; for example, models tend to underestimate the poleward heat transport in the North Atlantic [*Bryan*, 1982; *Bryan and Holland*, 1989; *Boning and Budich*, 1992].

The first goal of this study is to test the sigma - coordinate model, previously used only for modeling of coastal areas and estuaries, for a basin-scale problem. We want to compare the model calculations with calculations of simpler diagnostic models (i.e., Figure 1) and with calculations of other numerical models, with emphasis on issues concerning climate studies such as the meridional circulation and the heat transport in the ocean. The other goals of the paper are to demonstrate the model's dynamic behavior in adjusting the hydrographic data to topography and forcing and to study the physics of the adjustment process.

In section 2 the ocean model and numerical experiments are described. Then in section 3, results from the diagnostic and

prognostic calculations are discussed and compared with observations and other models. The dynamics of the adjustment process is discussed in section 4. Summary and conclusions are offered in section 5.

2. The Ocean Model

The Princeton ocean model used here is described in detail by *Blumberg and Mellor* [1987] and *Mellor* [1992]; it is a three-dimensional, free surface ocean model with a second - moment turbulence closure scheme [*Mellor and Yamada*, 1982] to provide vertical mixing coefficients. The model has been used, for example, in the study of bays and estuaries and in many process studies of coastal regions. Recently, modeling studies have focued on different aspects of the Gulf Stream system [*Mellor and Ezer*, 1991; *Oey et al.*, 1992; *Ezer and Mellor*, 1992, 1994; *Ezer et al.*, 1992, 1993; *Ezer*, 1994].

The prognostic variables of the model are the free surface η, potential temperature T, salinity S (hence density ρ), velocity components U,V, and W and turbulence energy and length scale. The initial T and S are obtained from the *Levitus* [1982] annual climatology data. The numerical scheme has a split time step, an external mode which solves the vertically integrated momentum equation, and an internal mode which solves the three-dimensional momentum equations. The horizontal diffusion uses the Smagorinsky formulation [*Smagorinsky et al.*, 1965], in which horizontal viscosity coefficients depend on the grid size and velocity gradients. The climatological mean temperature and salinity fields are subtracted before the horizontal diffusion is calculated, so artificial diapycnal mixing due to the along-sigma-level diffusion is minimized (see also *Mellor and Blumberg* [1985] for more detail on the horizontal diffusion formulation with sigma - coordinate systems). Bottom friction is formulated through the bottom boundary condition, wherein velocity is matched to the "law of the wall" by using a roughness parameter z_0 which varies from 1 cm in the deep ocean to 10 cm in the shallowest regions. However, except for the shallowest regions on the continental shelf, bottom boundary layers are not resolved with the current vertical resolution. Further details of the numerical model are given by *Blumberg and Mellor* [1987] and *Mellor* [1992] and in the papers mentioned above.

The vertical grid uses 15 sigma levels, where $\sigma = (z - \eta) / (H + \eta)$; σ ranges from $\sigma = 0$ at $z = \eta$ (at the surface) to $\sigma = -1$ at $z = -H$ (at the bottom). The horizontal grid uses a coast-following, curvilinear orthogonal system. Figure 2a shows the grid for every other grid point, and Figure 2b shows the bottom topography. The topography has been slightly smoothed in areas of steep topography to minimize truncation errors associated with sigma-coordinate models [*Haney*, 1991]; however, *Mellor et al.* [1994] show that these errors are almost completely eliminated by subtraction of the area mean density field before calculation of the pressure gradient terms in the model. Note that the resolution is much higher in the western Atlantic (20-30 km) than in the eastern Atlantic (80-100 km), so that the Gulf Stream, the Gulf of Mexico, and the east coast of the United States will be resolved. This is the main advantage of the irregular grid: computational resources are more efficiently used by increasing resolution in areas with strong gradients and minimizing the number of grid points over land.

The surface boundary conditions include heat flux and wind stress obtained from 2^{o}x2^{o} annually averaged climatologies of the Comprehensive Ocean-Atmosphere Data Set (COADS) analyzed by *Oberhuber* [1988]; the formulation of the surface forcing fields in the model are described in detail by *Ezer and Mellor* [1992]. Zero salinity fluxes are specified at the ocean surface. (For the diagnostic and short prognostic calculations here, surface heat and salt fluxes are not very significant.) The wind stress calculated from the COADS wind velocity using variable drag coefficient and the formulation used by *Ezer and Mellor* [1992] is consistent with that of *Hellerman and Rosenstein* [1983], which has been used in several other diagnostic models mentioned before.

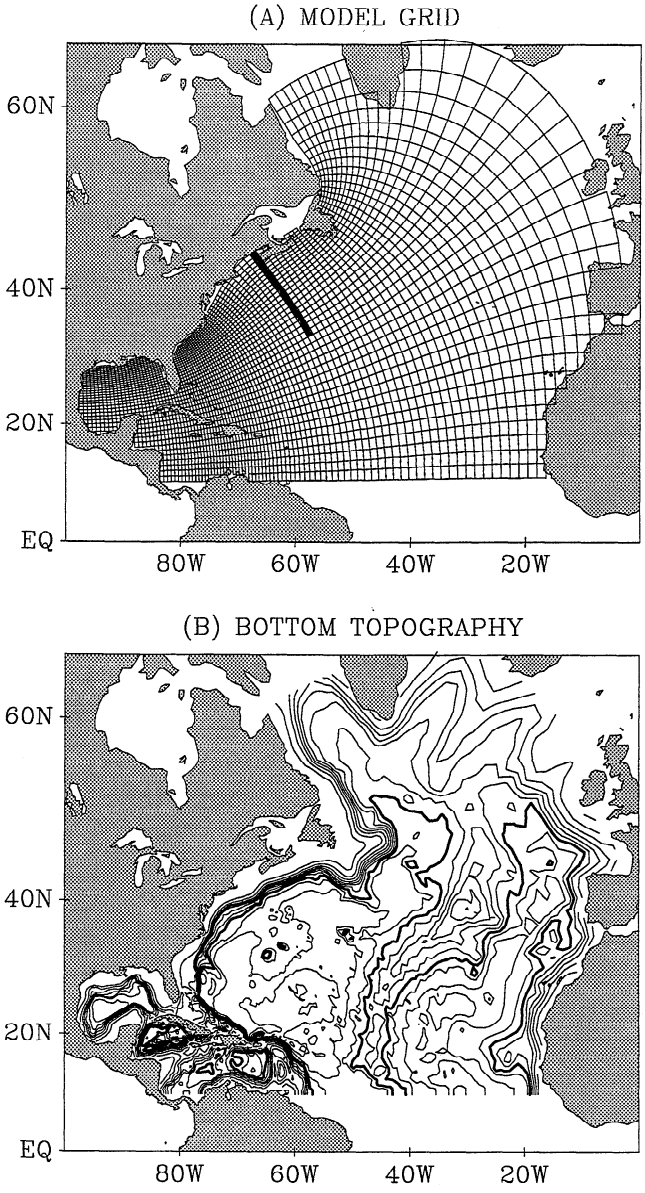

Figure 2. (a) The curvilinear orthogonal model grid. For clarity, only every other grid point is plotted. The thick line represents a cross section discussed in the legend to Figure 11. (b) The bottom topography of the model. The contour interval of the topography is 500 m; the thick line is the 4000-m contour.

The north and south open boundaries of the model are governed by the Sommerfeld radiation condition. Therefore although the total transport (the vertically averaged velocity perpendicular to the boundary) on the open boundaries is set to

zero, the internal velocities at each level are free to adjust geostrophically to the density field. Temperature and salinity on the open boundaries are locally upwinded, so under inflow conditions, prescribed climatological values are advected into the model domain. More detail on the open boundary conditions in the model can be found in the papers mentioned before.

3. Results from Diagnostic and Prognostic Calculations

3.1. Horizontal Circulation and Surface Elevation

The model was first run for 30 days in a purely diagnostic mode (holding T and S unchanged and equal to those in the Levitus data) and then continued in a prognostic mode. The surface elevation and the total stream function after 30 days of diagnostic calculations and after an additional 30 days of prognostic calculations are shown in Figure 3. Although the diagnostic calculation uses a computational algorithm very different from the one in the *Mellor et al.* [1982] model (based on (1)), Figures 1 and 3c are quite similar. The structures of the subtropical gyre and the subpolar gyre, including the recirculation gyres on both sides of the Gulf Stream and the anticyclonic circulation over the Mid-Atlantic ridge are similar in both calculations. Subtropical regions are quite noisy in both cases. Here, however, the northern recirculation gyre off Nova Scotia is somewhat weaker than the more realistic gyre described by *Mellor et al.* [1982]. This gyre north of the Gulf Stream may play a crucial role in maintaining Gulf Stream separation at Cape Hatteras in numerical models [*Ezer and Mellor*, 1992]. The diagnostic surface elevation after 30 days shows a realistic 1-m change across the Gulf Stream (Figure 3a), but the Gulf Stream is too wide (about 400 km), a reflection of the overly smoothed Levitus climatology. Experiments (not shown) with different horizontal resolutions show only insignificant differences in the diagnostic circulation, a result of the large-scale averaging of the Levitus data; however, prognostic calculations (described below) are more sensitive to model resolution.

The fields after 60 days (30 days diagnostic and 30 days prognostic) are shown in Figures 3b and 3d; they are very similar to those after 90 days (a discussion of the adjustment time - scale is given later). During the prognostic calculation, surface elevation does not change much (Figure 3b), but the total stream function shows a more organized flow in the subtropical region, through the Caribbean Sea, and into the Gulf of Mexico (Figure 3d). The fact that the flow is less noisy after the short prognostic run indicates that noise due to errors in the hydro-

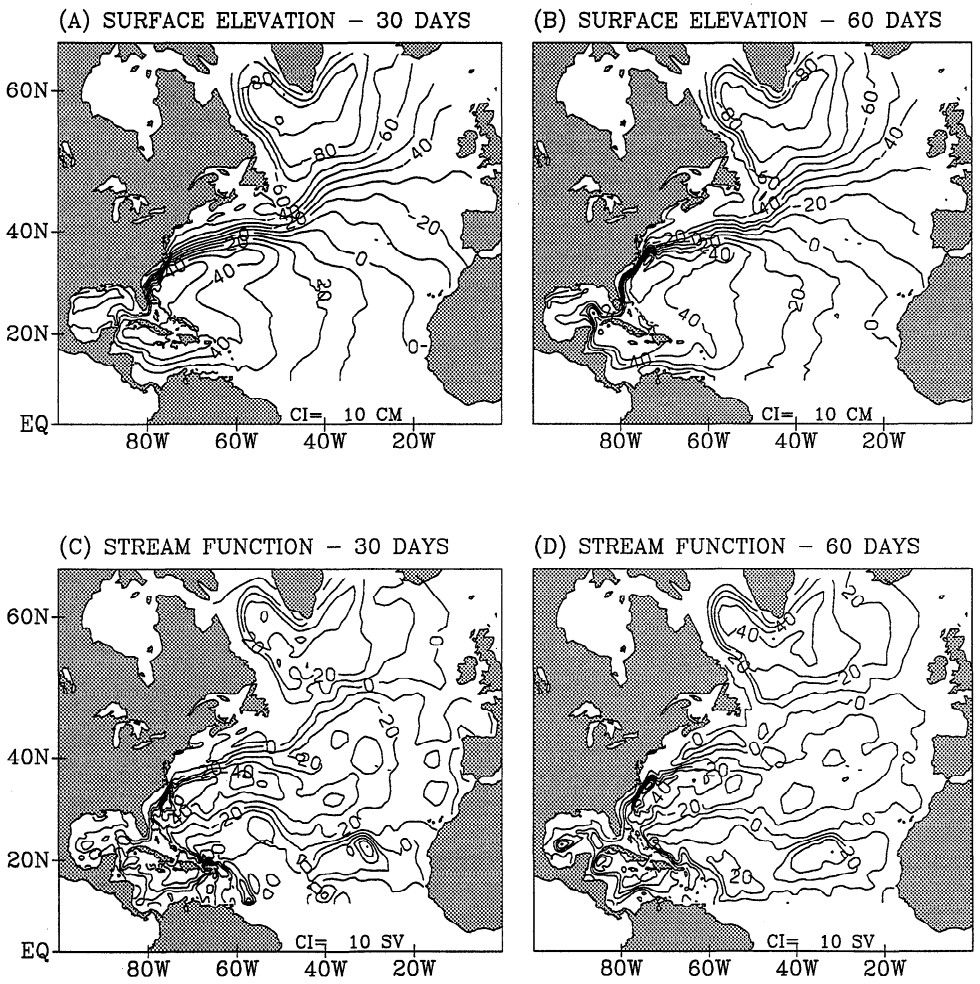

Figure 3. Surface elevation (a) after 30 days of diagnostic run and (b) after an additional 30 days of prognostic run, with contour interval of 10 cm; vertically integrated total stream function (c) after 30 days of diagnostic run, and (d) after an additional 30 days of prognostic runs, with contour interval of 10 Sv.

graphic data or inconsistencies between the data and the bottom topography, as suggested by *Sarmiento and Bryan* [1982], is removed by advection and diffusion. Generally, the comparison with the simpler model used by *Mellor et al.* [1982] and *Greatbatch et al.* [1991] shows that the simple model is capable of producing the essence of the North Atlantic circulation, though some of the smaller circulation patterns in the latter model may be associated with noise because of data inconsistencies.

3.2. Coastal Sea Level

The model used here is a general circulation ocean model as well as a coastal ocean model, and provides a dynamic connection between the general circulation of the deep ocean and variations of coastal sea level. According to previous model calculations, temporal variations in coastal sea level due to mesoscale activity of the Gulf Stream are of the order of 10 cm [*Mellor and Ezer*, 1991; *Oey et al.*, 1992]. While long-term records of coastal sea level may provide an indicator of climate change, those records may also include large spatial and temporal variations associated with changes in the open-ocean circulation. It is a difficult task to measure the spatial changes of sea level along the coast; for example, *Sturges* [1968] suggested that the sea level obtained by a geodetic leveling method was inconsistent with the observed Gulf Stream flow. Geopotential calculations using hydrographic data may give a better estimate of coastal sea level, but they cannot apply directly to the continental shelf [*Sturges* 1974]. On the other hand, with the aid of a free surface coastal ocean model, those variations can be modeled.

The coastal sea level in the model is defined as the model sea surface height near the closed boundaries (i.e., at 10-m depth on the continental shelf). Figure 4a shows the coastal sea level change along the North America coast derived from the diagnostic and prognostic calculations and forced by the annual mean winds. Estimates of steric sea level from different sources, summarized by *Sturges* [1974], yield an 80-cm drop in sea level along the western continental boundary of the North Atlantic from the equator to 40°N. Our model calculations produce very similar results (Figure 4a). Moreover, the model calculations here show much more detailed information than can be gained by observation. The change in coastal sea level reflects boundary current dynamics, wind stress, and variations in the coastline. Note, for example, the large drop in sea level between the Florida Straits and Cape Hatteras and downstream of Cape Hatteras. The intensification of the Gulf Stream there must be supported by an increasing sea surface gradient across the Gulf Stream and consequently a downstream sea level drop, as was previously shown by observations and models [*Oey et al.*, 1992]. Note also the sudden change of sea level where the coastline changes (e.g., Cape Hatteras and Newfoundland) and in straits (e.g., Yucatan and Florida Straits). The increasing sea level at high latitude is evident also in observations [*Sturges*, 1974] and is probably related to the southward flow of the Labrador Current. The sea level after 90 days (not shown) does not differ significantly from that after 60 days.

Figure 4b shows the difference between the sea level obtained from the above run with annual wind forcing and that obtained from a run with zero wind forcing. The direct effect of the wind is to increase sea level at low latitudes by almost 10 cm and decrease sea level at high latitudes by as much as 17 cm at 40°N. This is a result of the local wind effect in those regions and the wind-driven component of the deep ocean transport. *Greatbatch et al.* [1990] simulate the coastal sea level on the Newfoundland and Labrador shelf and try to separate local and remote effects. Their study shows that the contribution to coastal sea level from the open ocean circulation may be more significant in some regions than in others.

3.3. Velocity Fields

The velocity fields before and after the prognostic calculation are shown in Figures 5 and 6, for 50 m and 2500 m, respectively. After 30 days of diagnostic calculation (Figure 5a), the flow at 50 m shows a fairly realistic Gulf Stream and Labrador Current but noisy and unorganized flow elsewhere, with especially strong velocities in the Caribbean Sea. After an additional 30 days of prognostic calculation (Figure 5b), much of the noisy flow in the interior disappears, and a more realistic western boundary current through the Caribbean and the loop current in the Gulf of Mexico and into the Gulf Stream are now apparent. Similarly, the deep flow at 2500 m changes by the prognostic calculation from noisy and unorganized flow field (Figure 6a) into a more coherent deep flow pattern (Figure 6b) with the Deep Western Boundary Current (DWBC) flowing southward along the continent from the Labrador Sea into the equatorial region. Some of the deep flows that remain in the interior (e.g., at 30°W, 20°N) seem to follow the isobaths of the Middle Atlantic Ridge.

The interpretation of the change in the horizontal velocity fields from the diagnostic to the prognostic calculation is that sampling errors and inconsistencies between the hydrography and bottom topography produce erroneous velocities in the diagnostic calculation. However, advection and diffusion in the prognostic calculation restore the dynamical balance that is consistent with large-scale ocean circulation, which is still governed by the coarse-resolution hydrographic data. For example, the general structure of the temperature field after 60 days (not shown) is very similar to that of the initial field except for small, random-looking changes of the order of 0.1° to 0.5°C at many grid points. In the interior the vertical velocity field (not shown) also indicates a random-looking noise with values in the diagnostic calculation 1 order of magnitude larger than those in the prognostic calculation.

3.4. Meridional Circulation and Heat Transport

Important processes in climate studies are deep water formation at high latitudes and meridional heat transfer between high and low latitudes as inferred from the zonal mean meridional circulation. *Hall and Bryden* [1982] measured as much as 1.2 PW (1 PW = 10^{15} W) of poleward heat transport in the North Atlantic, while *Isemer et al.* [1989] estimated the latitudinal variations in poleward heat transport based on air-sea fluxes; the latter calculations were constrained to 1 PW at 24°N. Ocean models and inverse calculations with ocean models tend to have a relatively weak thermohaline circulation and thus often estimate poleward heat transport with a maximum value around 0.5-0.8 PW [*Bryan*, 1982; *Manabe and Stouffer*, 1988; *Bryan and Holland*, 1989; *Böning and Budich*, 1992; *Tziperman et al.* 1992; *Marotzke and Wunsch*, 1993]. All the above studies use different versions of the Bryan-Cox z - level model. Recent studies indicate that neither optimizing the surface heat fluxes [*Tziperman and Bryan*, 1993] nor increasing the horizontal resolution [*Beckmann et al.*, 1994] led to improvement in the model heat transport. However, new studies have indicated that

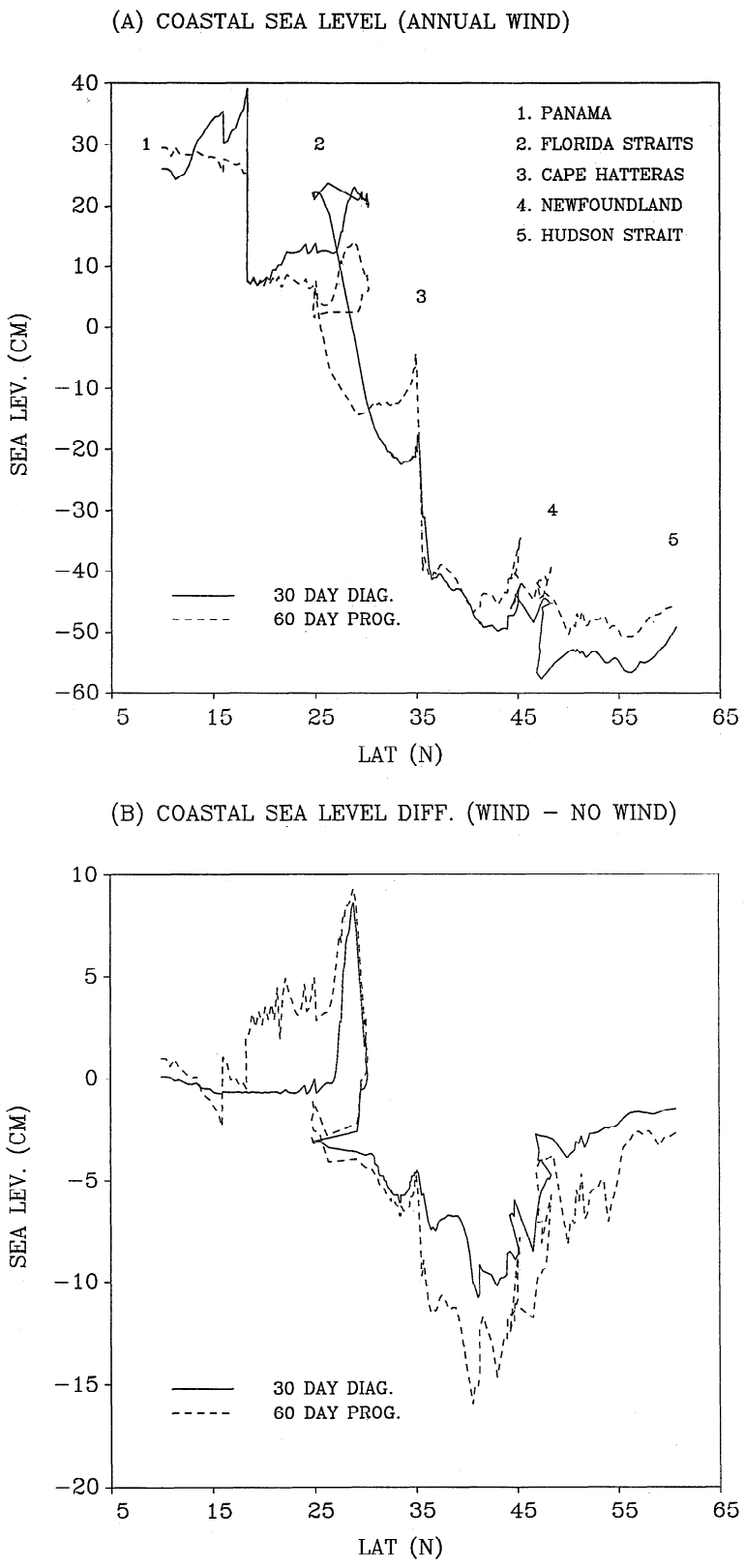

Figure 4. (a) Coastal sea level along the North American continent obtained from the diagnostic (30 days) and prognostic (60 days) calculations with annual wind forcing. Five selected locations along the coast are indicated in (a). (b) The sea level difference between the run with annual winds and the run with zero winds. Sea levels after 30 and 60 days are indicated by solid and dashed curves respectively.

inaccurate temperatures imposed at high latitudes (R. Gerdes, personal communication 1994) and formulation of the horizontal mixing (C.W. Böning , personal communication 1994) may be partly to blame for the model deficiencies. In any case, it is interesting to see if the sigma - level model suffers from the same problem.

In our curvilinear grid, an accurate integration across the basin is done by summing fluxes calculated by the model on the

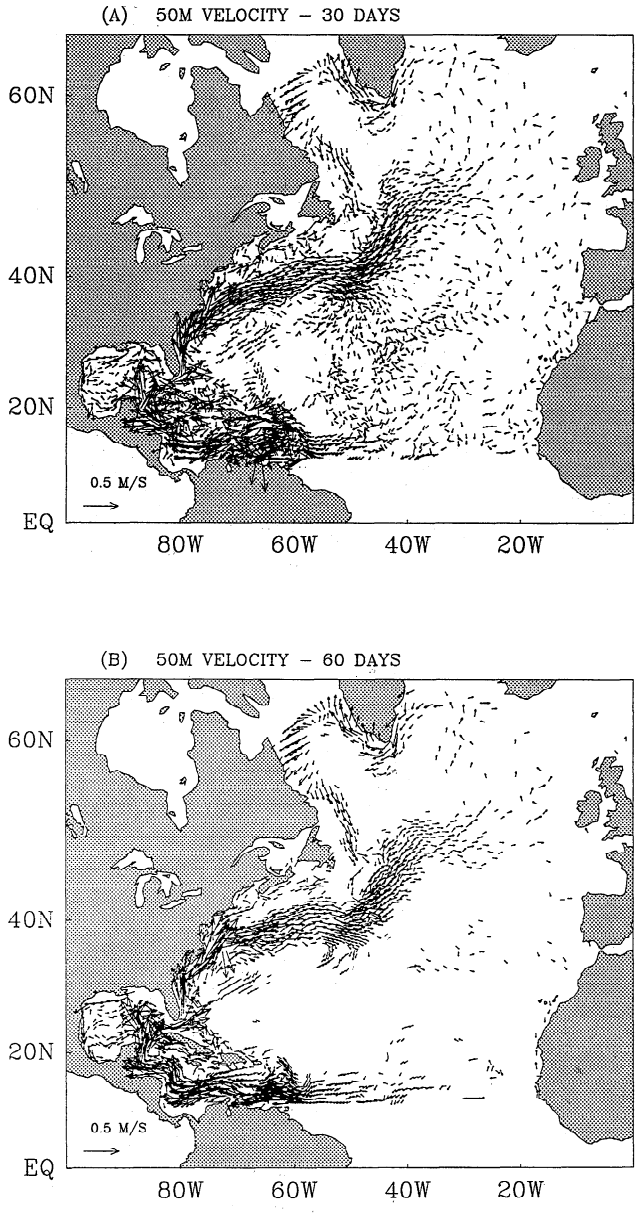

Figure 5. Velocity vectors at depth of 50 m (a) after 30 days of diagnostic calculation and (b) after an additional 30 days of prognostic calculation. The vector at the bottom left corner indicates the largest arrow that is plotted; velocities larger than the indicated value (0.5 m s^{-1}) are truncated to the size of this vector; velocities smaller than 10% of this value (0.05 m s^{-1}) are not plotted.

model grid; this results in a zigzag contour around an average latitude circle. The results for 30 and 60 days are shown in Figures 7a and 7b, respectively. Although the diagnostic calculation shows reasonable horizontal general circulation patterns (Figures 3a and 3c), the diagnostic meridional circulation of Figure 7a is very noisy and unrealistic. This is consistent, however, with similar results obtained by *Sarmiento and Bryan* [1982] and *Tziperman et al.* [1992], using the same *Levitus* [1982] data set used here; thus this noise is inherent in the data and is not a result of the model type.

The meridional circulation after 60 days as shown in Figure 7b is, however, more reasonable. (The meridional circulation after 1 year is almost the same but will probably change for longer simulations with more realistic forcing.) The ~20-Sv transport of the overturning cell at 60°N is quite realistic, but the southward deep flow near the southern boundary at 10°N is too weak owing to the effect of the model boundary condition. Experiments (not shown) with different open-boundary conditions indicate possible improvement of the flow near the boundary but have little effect on the interior circulation, which is dominated by the density fields and surface wind forcing.

The thermohaline circulation in Figure 7b produces a poleward flow of warm water in the upper ocean and an equatorward flow of cold water in the deep ocean, thus a net positive heat transport in the North Atlantic, as shown in Figure 8. Also shown (heavy curve) is the heat transport estimated by *Isemer et al.* [1989] on the basis of observed air-sea fluxes and direct oceanic measurements. Note again that the purely diagnostic calculation gives a very noisy and unrealistic heat flux (Figure 8a), owing to the noisy flow field discussed before. After a 30-

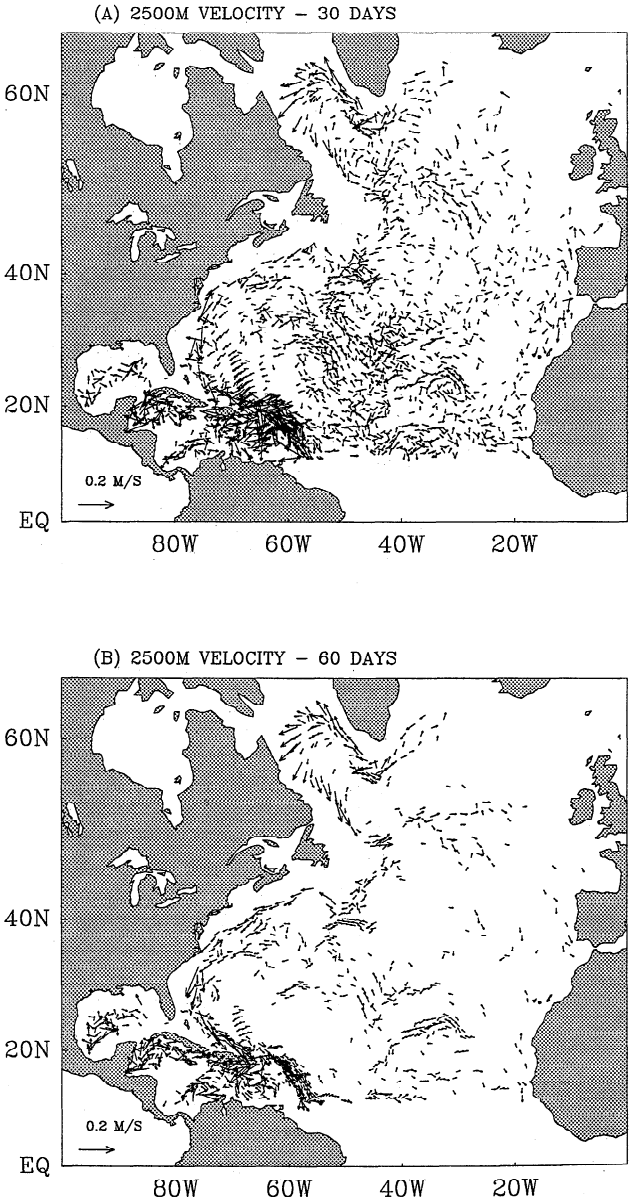

Figure 6. Same as Figure 5 but for velocity vectors at 2500 m. The scale for the maximum vector is 0.2 m s^{-1}, and velocities smaller than 0.02 m s^{-1} are not plotted.

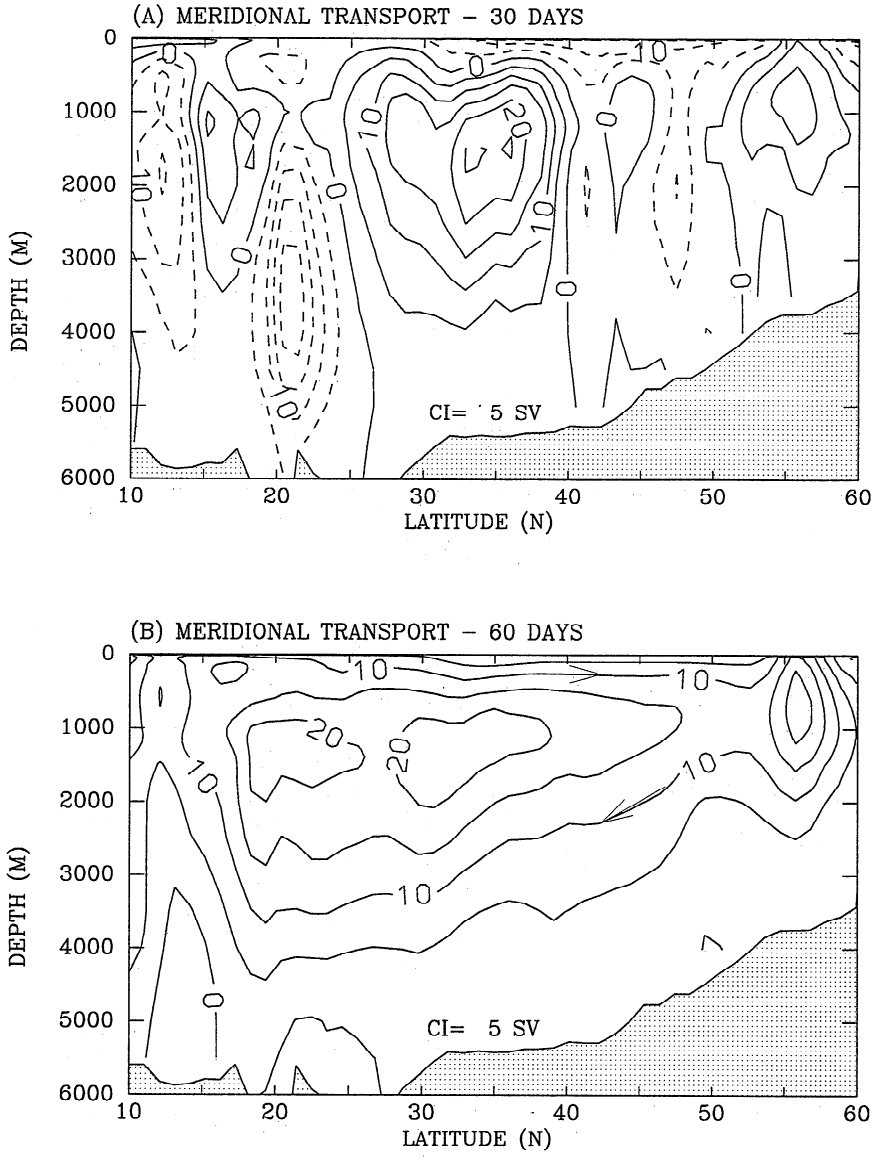

Figure 7. Meridional (zonally averaged) stream function (a) after 30 days of diagnostic calculation, and (b) after an additional 30 days of prognostic calculation. Contour interval (CI) is 5 Sv; dashed curves represent negative values.

day prognostic run, flow fields are adjusted, and the heat transport agrees quite well with the observed transport (Figure 8b); with further diagnostic calculation up to day 180 (Figure 8c), model calculations improve even more. Near the south boundary, model heat transport is too small because of the imposed boundary condition. At middle latitudes the model gives heat transport values of up to 1.2 PW, which is somewhat larger than those of *Isemer et al.* [1989] but very similar to the values estimated from the measurements reported by *Hall and Bryden* [1982].

4. Dynamics of the Adjustment Process

The adjustment process from the initial state to the diagnostic and prognostic states is shown in the changes of volume-averaged mean kinetic energy (Figure 9); the calculations made without considering wind are also included for comparison. The decrease in mean kinetic energy after the switch to the prognostic calculation (after 30 days) indicates removal of noise from the initial hydrographic data (as seen before, for example, in Figures 5, 6, 7, and 8) by advection and diffusion and the dynamic adjustment of the flow to the bottom topography and wind. The adjustment seems very fast, with an e-folding time scale of about 5 days. The effect of the wind is, as expected, larger at the surface layer (the sigma layer is 0.002 the thickness of the water depth) (Figure 9a) where the kinetic energy is reduced by a factor of 4 when winds are neglected. A negligible wind effect can be seen at the bottom layer (the sigma layer is 0.125 the thickness of the water depth) (Figure 9b).

In the previous sections, we have discussed how the model dynamics are used to adjust the observed density field to topography and forcing. Now we look in more detail into the dynamics of the adjustment process by analyzing the temporal and spatial variations of the terms of the vertically integrated vorticity balance equation. The momentum equations for the vertically averaged velocity components (indicated by the overbars) can be written as follows:

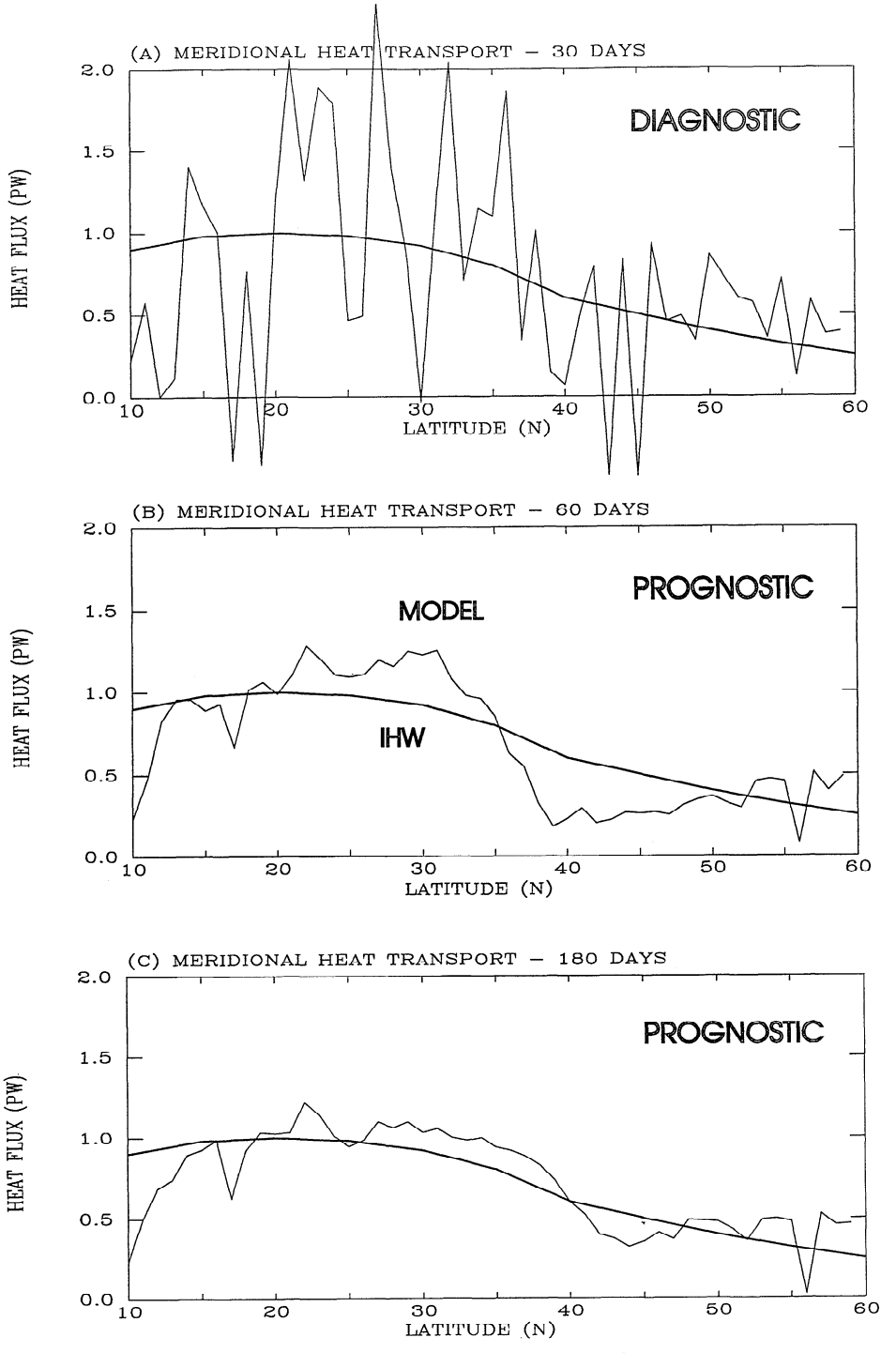

Figure 8. Poleward meridional heat transport (in petawatts) (1 PW=10^{15}W) as a function of latitude after (a) 30 days (diagnostic), (b) 60 days and (c) 180 days. Thin curves represent the model calculations; heavy curves (indicated by IHW) are from *Isemer et al.* [1989].

$$\frac{\partial \bar{u}D}{\partial t} + A_x - f\bar{v}D = -Dg\frac{\partial \eta}{\partial x} - \tilde{\Phi}_x + \tau_{x0} - \tau_{xb} \tag{2a}$$

$$\frac{\partial \bar{v}D}{\partial t} + A_y - f\bar{u}D = -Dg\frac{\partial \eta}{\partial y} - \tilde{\Phi}_y + \tau_{y0} - \tau_{yb} \tag{2b}$$

where A_x and A_y are horizontal advection and diffusion terms, respectively, and τ_{x0}, τ_{y0} are surface stress terms, and τ_{xb}, τ_{yb} are bottom stress terms. The pressure gradient terms are

$$\tilde{\Phi}_x \equiv \int_{-H}^{\eta}\int_{z}^{\eta}\frac{\partial b'}{\partial x}\,dz'\,dz \tag{3a}$$

$$\tilde{\Phi}_y \equiv \int_{-H}^{\eta}\int_{z}^{\eta}\frac{\partial b'}{\partial y}\,dz'\,dz \tag{3b}$$

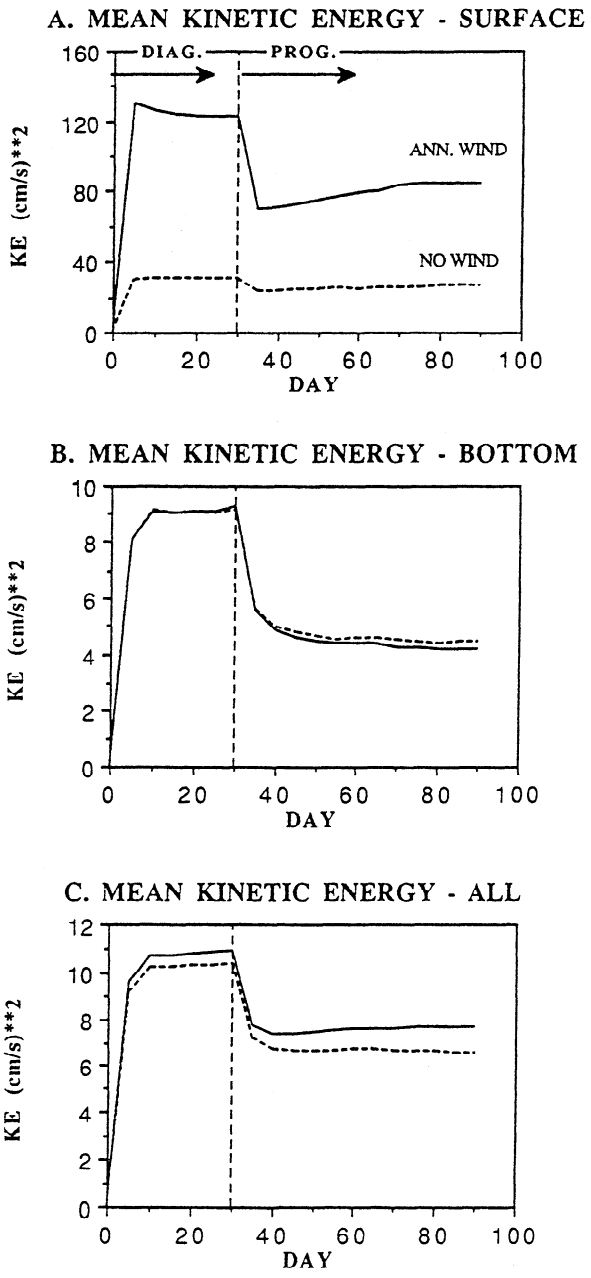

Figure 9. The volume-averaged mean kinetic energy as a function of time for the model forced with annual winds (solid curves) and with no winds (dashed curves). (a) Surface layer; (b) bottom layer; (c) all layers.

where $b=\rho g$ is the buoyancy. It can be shown that

$$\tilde{\Phi}_x + Dg\frac{\partial \eta}{\partial x} = \frac{\partial \Phi}{\partial x} + D\frac{\partial P_b}{\partial x},$$

$$\tilde{\Phi}_y + Dg\frac{\partial \eta}{\partial y} = \frac{\partial \Phi}{\partial y} + D\frac{\partial P_b}{\partial y}$$

where

$$\Phi = \int_{-H}^{\eta} z\, b\, dz$$

is the potential energy and

$$P_b = g\eta + \int_{-H}^{\eta} b\, dz$$

is the bottom pressure.

Now, cross-differentiate (2a) and (2b) to obtain the vertically integrated vorticity balance equation

$$\frac{\partial}{\partial t}\left(\frac{\partial \bar{v}D}{\partial x} - \frac{\partial \bar{u}D}{\partial y}\right) + \frac{\partial A_y}{\partial x} - \frac{\partial A_x}{\partial y} + \frac{\partial (f\bar{u}D)}{\partial x} + \frac{\partial (f\bar{v}D)}{\partial y} = \frac{\partial P_b}{\partial x}\frac{\partial D}{\partial y} - \frac{\partial P_b}{\partial y}\frac{\partial D}{\partial x} + \frac{\partial (\tau_{y0} - \tau_{yb})}{\partial x} - \frac{\partial (\tau_{x0} - \tau_{xb})}{\partial y} \quad (4)$$

On the left side of (4) are the tendency term, advection and diffusion terms, and Coriolis term. On the right side are the bottom pressure torque term and the surface and bottom stress curl terms. For steady flow, $\partial(\bar{u}D)/\partial x + \partial(\bar{v}D)/\partial y = 0$, and the Coriolis-dominated term becomes the beta term $\beta \bar{v} D$, where $\beta = \partial f/\partial y$. In the numerical implementation of (4), the vorticity is calculated, using Stokes theorem, by taking a line integral of (2a) and (2b) around each grid cell and then dividing by the area of the cell. First, the temporal variations of the terms in (4) are discussed, and then their spatial distributions are discussed.

Figure 10 shows the average (over the entire model domain) absolute values of the terms in (4); these simulations include 30 days of diagnostic calculation followed by 150 days of prognostic calculation. Advection and diffusion terms are combined together here, as is done in the numerical model. However, here advection is about 1 order of magnitude larger than diffusion (when integrating over the model domain); diffusion will become more significant, though, in a model with coarser resolution, as a grid-dependent horizontal diffusion is used in the model. The adjustment after the prognostic calculation starts is characterized by two different time scales. The first scale is a short timescale (about 10 days) of fast adjustment of the flow field to forcing and topography and the relaxation of fast-moving barotropic waves. Note the large change in the amplitude of the bottom pressure torque term after 30 days (curve 4 in Figure 10). The second scale is a long timescale (months and possibly several years), indicated by the tendency term (curve 6 in Figure 10). The long timescale is due mostly to the relaxation of baroclinic Rossby waves propagating across the basin and slow advection in the deep layers. Note that Figure 10 shows only the area-averaged absolute value of each term; however, at each model grid cell the terms may have positive or negative values and add up to zero. The local balance is discussed later in more detail. The magnitude of the terms indicates that the flow is dominated by topography, as the largest term is the bottom pressure torque term. The magnitudes of the wind stress and the bottom stress terms are comparable to each other but smaller than the magnitudes of

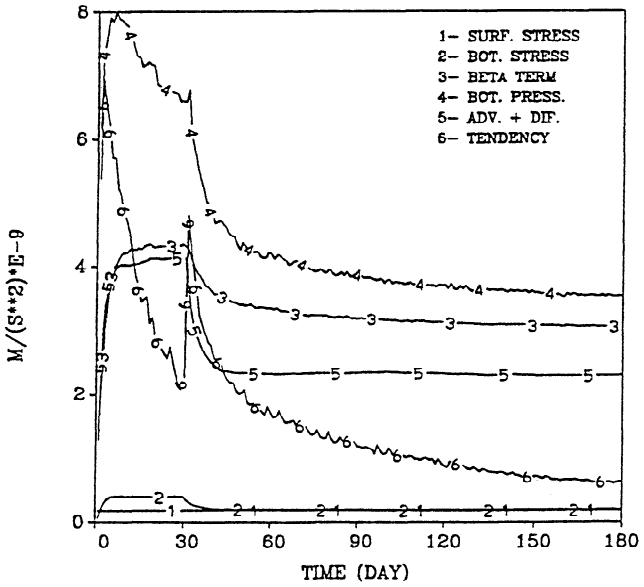

Figure 10. The change with time of the absolute values of the terms of the vorticity balance equation (4) averaged over the model domain. The terms are noted as follows: 1, surface stress; 2, bottom stress; 3, beta term; 4, bottom pressure torque; 5, advection and diffusion; 6, tendency. The first 30 days are the diagnostic calculations.

the other terms. While the classical Sverdrup balance $\beta \bar{V} D$ = curl (τ_0) prevails in some regions in the interior of the domain, the magnitude of the terms here is dominated by topography and western boundary current dynamics.

An example of the balance of the dominant terms across the continental slope and across the Gulf Stream (in the cross section indicated in Figure 2a) is plotted in Figures 11a and 11b for 30 days and 60 days of calculations (after 180 days the distribution is quite similar to that in Figure 11b). Only the beta term, the bottom pressure torque, and the advection and diffusion term (actually this term is dominated by advection) are shown; the magnitudes of the other terms (not shown in Figure 11) are at least an order of magnitude smaller in this region. All terms are larger and noisier during the diagnostic calculation, with the consequences, shown before, of noisy horizontal and vertical velocity fields, and large eddy kinetic energy. After 60 days, terms are especially large in three distinct regions (going from right to left in Figure 11b) which are controlled by different processes: the continental slope, the Gulf Stream, and areas near topographic features in the deep ocean. On the continental slope, where the flow follows the bathymetry, the dominant terms with similar amplitudes are the bottom pressure term, the advection term, and the beta term. This flow includes the deep western boundary current and the northern recirculation gyre north of the Gulf Stream. Near the Gulf Stream, the strong flow is indicated by the large beta term, which is balanced by horizontal advection (which is large there owing to the large velocities in the Gulf Stream). Topographic features in the deep ocean (e.g., the peaks at 1000-km distance are near the New England Seamount Chain) cause an increase in the bottom pressure torque which is balanced by the beta term. The intensification of the flow and the meandering of the Gulf Stream due to the effects of the New England Seamounts have been recently simulated by *Ezer* [1994]. The balances seem complicated and region dependent; however, other cross sections indicate patterns similar to those of Figure 11.

5. Discussion and Conclusions

The first goals of this study were to derive ocean circulation from hydrographic and wind stress data, using the primitive equation, sigma - coordinate Princeton ocean model, and to compare the circulation thus derived with that derived by simpler diagnostic methods and other models. This is the first test of this model for basin-scale problems; it has been used before primarily for coastal regions and estuaries. The second goal was to study the process of adjustment of density and flow fields from initial conditions obtained from climatological hydrography data; this initialization has become a standard for most numerical ocean simulations.

The comparison between this model, which uses the full nonlinear, primitive equation formulation, and the simpler diagnostic model, based on (1), used by *Mellor et al.* [1982] and *Greatbatch et al.* [1991] shows that the general horizontal circulations of the two schemes are quite similar. However, coastal regions and regions with complicated topographies that could not be resolved before are now included in the calculation. The simple diagnostic models are based on vertically averaged dynamics and thus could not produce the vertical detail of the flow. A problem that arises, however, is that the purely diagnostic calculation (keeping the density field unchanged and equal to that in the Levitus data) produces an unphysical meridional circulation and heat transport. Similar results of other studies [*Sarmiento and Bryan*, 1982; *Tziperman et al.*, 1992] suggest that this is the result of inconsistencies between the hydrographic data and the bottom topography rather than a result of problems associated with a particular model. While other diagnostic models use techniques such as filtering the data, adding damping terms to the prognostic equations, or using inverse optimization to correct this problem, here we use a dynamic approach in which short prognostic runs following the diagnostic calculations are used to correct the density field. In this method (described also by *Demin et al.*. [1990]) the large-scale ocean circulation remains unaffected, while only small-scale noise is removed. The results show a rapid dynamic adjustment (in about 10-30 days) of the density fields, yielding narrower boundary currents, more realistic velocity fields, and consequently meridional circulation consistent with results obtained by other models. The use of model dynamics through short prognostic calculations to obtain a flow field consistent with topography and forcing has some advantages over optimization techniques [*Wunsch*, 1978; *Tziperman et al.*, 1992; *Marotzke and Wunsch*, 1993], which may require simplification of the dynamics and the use of coarse-resolution models owing to the large computational load of inverse methods.

One of the major findings of the study is that even the overly smoothed *Levitus* [1982] data set contains much information about the thermohaline circulation, and after some inconsistencies and noise are removed, realistic meridional circulation with about 20-Sv transport in the overturning cell and realistic poleward heat transport with a maximum value of about 1.2 PW are produced by the model. The difference between our results with the sigma - coordinate model and pervious simulations with z - level models, which often estimate relatively weaker thermohaline circulation, can be attributed to several differences in the numerical techniques and parameterization. For example, sigma-level models may resolve bottom

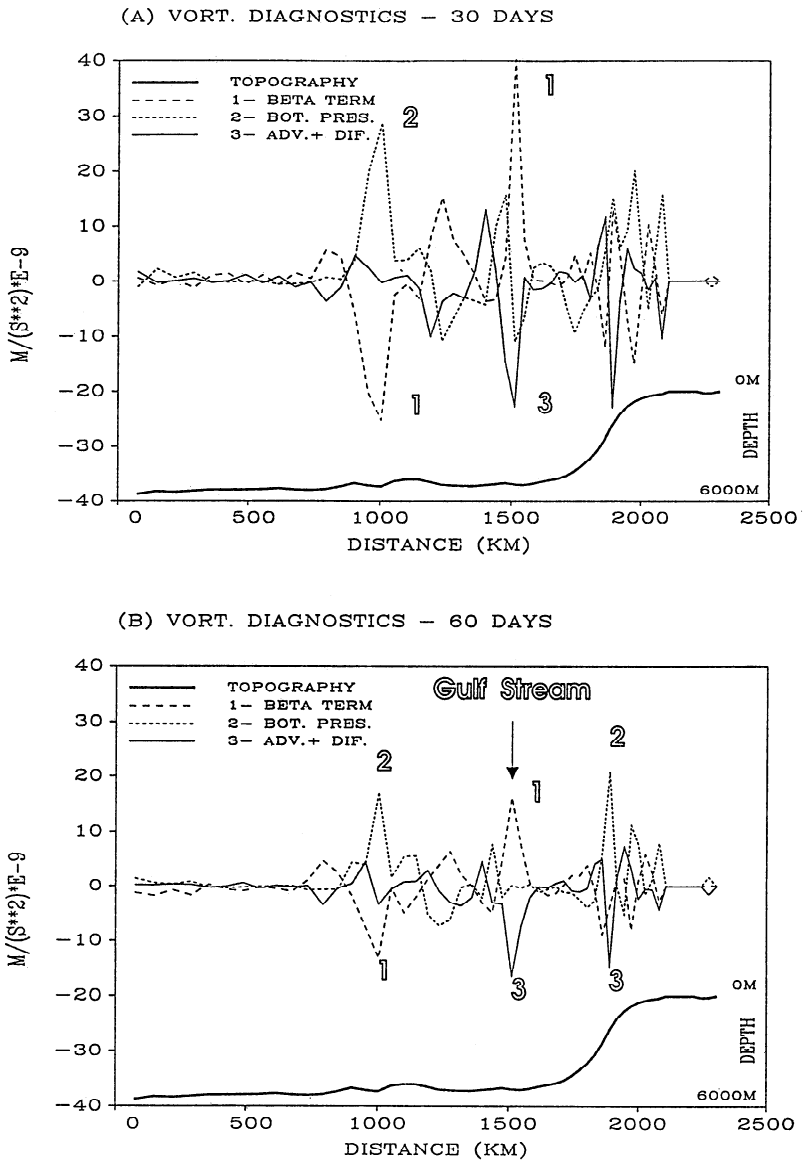

Figure 11. The spatial distribution of the leading terms of the vorticity balance equation. (a) After 30 days of diagnostic calculation and (b) after an additional 30 days of prognostic calculation. The cross section, indicated in Figure 2a, is from south to north along the curvilinear model grid. The beta term, the bottom pressure torque, and the advection and diffusion term are indicated by dashed (curve 1), dotted (curve 2), and solid (curve 3) curves, respectively; bottom topography is indicated by the thick line.

topography better than z - level models [Gerdes, 1993]; parameterization of horizontal and vertical mixing and open boundary conditions are also different in each model.

The technique used here will be used in the future for studies of climate change. For example, one can extend and verify the results of *Greatbatch et al.* [1991] concerning the dramatic changes in circulation between the pentads 1955-1959 and 1970-1974, by using the Levitus data for those periods. Longer simulations for climatological time scales are planned, and the altimetric data assimilation technique of *Mellor and Ezer* [1991] and *Ezer and Mellor* [1994], which has been used with this model for nowcasting the Gulf Stream region, will be extended to the entire Atlantic Ocean.

Acknowledgments. We thank the reviewers for useful suggestions. The research was supported by Office for Naval Research (Navy Ocean Modeling and Prediction Program) grant N00014-93-1-0037, NOAA's National Ocean Service, NOAA's Atlantic Climate Change Program grant NA36GP0262, and NOAA's Geophysical Fluid Dynamics Laboratory.

References

Beckmann, A., C. W. Boning, C. Koberle, and J. Willebrand, Effects of increased horizontal resolution in a simulation of the North Atlantic ocean, *J. Phys. Oceanogr., 24*, 326-344, 1994.

Blumberg, A. F., and G. L. Mellor, A description of a three-dimensional coastal ocean circulation model, in *Three-Dimensional Coastal Ocean Models, Coastal Estuarine Sci.*, vol., 4, edited by N. Heaps., pp. 1-16, AGU, Washington, D.C., 1987.

Böning, C. W., and R. G. Budich, Eddy dynamics in a primitive equation model: Sensitivity to horizontal resolution and friction, *J. Phys. Oceanogr., 22*, 361-381, 1992.

Bryan, F., and W. R. Holland, A high-resolution simulation of the wind

and thermohaline-driven circulation of the North Atlantic Ocean, in *Aha Huliko'a, The Proceedings of the Hawaiian Winter Workshop,* pp. 99-116, University of Hawaii, Honolulu, 1989.

Bryan, K., Poleward heat transport by the oceans: Observations and models, *Annu. Rev. Earth Planet. Sci., 10,* 15-38, 1982.

Demin, Y. L., H. J. Friedrich, R. A. Ibraiv, A. S. Sarkisyan, and J. Sundermann, A note on modelling the world ocean climate, *Ocean Modell., 89,* pp. 10-11, Hooke Inst. Oxford, England, 1990.

Ezer, T., On the interaction between the Gulf Stream and the New England seamount chain, *J. Phys. Oceanogr., 24,* 191-204, 1994.

Ezer, T., and G. L. Mellor, A numerical study of the variability and the separation of the Gulf Stream induced by surface atmospheric forcing and lateral boundary flows, *J. Phys. Oceanogr., 22,* 660-682, 1992.

Ezer, T., and G. L. Mellor, Continuous assimilation of Geosat altimeter data into a three-dimensional primitive equation Gulf Stream model, *J. Phys. Oceanogr., 24,* 832-847, 1994.

Ezer, T., D.-S. Ko, and G. L. Mellor, Modeling and forecasting the Gulf Stream, *Mar. Technology Soc. J., 26*(2), 5-14, 1992.

Ezer, T., G. L. Mellor, D.-S. Ko, and Z. Sirkes, A comparison of Gulf Stream sea surface height fields derived from Geosat altimeter data and those derived from sea surface temperature data, *J. Atmos. Oceanic Technol., 10,* 76-87, 1993.

Fujio, S., T. Kadowaki, and N. Imasato, World ocean circulation diagnostically derived from hydrographic and wind stress fields, 1, The velocity field, *J. Geophys. Res., 97,* 11,163-11,176, 1992.

Gerdes, R., A primitive equation ocean circulation model using a general vertical coordinate transformation, 1, Description and testing of the model, *J. Geophys. Res., 98,* 14,683-14,701, 1993.

Greatbatch, R. J., B. de Young, A. D. Goulding, and J. Craig, On the influence of local and North Atlantic wind forcing on the seasonal variation of sea level on the Newfoundland and Labrador shelf, *J. Geophys. Res., 95,* 5279-5289, 1990.

Greatbatch, R. J., A. F. Fanning, A. D. Goulding, and S. Levitus, A diagnosis of interpentadal circulation changes in the North Atlantic, *J. Geophys. Res., 96,* 22,009-22,023, 1991.

Hall, M. M., and H. L. Bryden, Direct estimates and mechanisms of ocean heat transport, *Deep Sea Res., 29,* 339-359, 1982.

Haney, R. L., On the pressure gradient force over steep topography in sigma-coordinate ocean models, *J. Phys. Oceanogr., 21,* 610-619, 1991.

Hellerman, S., and M. Rosenstein, Normal monthly wind stress over the world ocean with error estimates, *J. Phys. Oceanogr., 13,* 1093-1104, 1983.

Hogg, N. G., R. S. Pickart, R. M. Hendry, and W. J. Smethie, The northern recirculation gyre of the Gulf Stream, *Deep Sea Res., 33,* 1139-1165, 1986.

Holland, W. R., Baroclinic and topographic influences on the transport in western boundary currents, *Geophys. Fluid Dyn., 4,* 187-210, 1973.

Holland, W. R., and A. Hirschman, A numerical calculation of the circulation in the North Atlantic Ocean, *J. Phys. Oceanogr., 2,* 336-354, 1972.

Isemer, H. J., J. Willebrand, and L. Hasse, Fine adjustment of large scale air-sea energy flux parameterization by a direct estimate of ocean heat transport, *J. Clim., 2,* 1173-1184, 1989.

Kantha, L. H., G. L. Mellor, and A. F. Blumberg, A diagnostic calculation of the seneral circulation in the South Atlantic Bight, *J. Phys. Oceanogr., 12,* 805-819, 1982.

Levitus, S., Climatological atlas of the world ocean, *NOAA Prof. Pap. 13,* 173 pp. U.S. Govt. Print. Office, Washington, D. C., 1982.

Manabe, S., and R. J. Stouffer, Two stable equilibria of a coupled ocean-atmosphere model, *J. Clim., 1,* 841-866, 1988.

Marotzke, J., and C. Wunsch, Finding the steady state of a general circulation model through data assimilation: Application to the North Atlantic ocean, *J. Geophys. Res., 98,* 20,149-20,167, 1993.

Mellor, G. L., User's guide for a three-dimensional, primitive equation, numerical cean model, *Program in Atmospheric and Oceanographic Sciences Report,* 35 pp. Princeton University, Princeton, N.J., 1992.

Mellor, G. L., and A. F. Blumberg, Modeling vertical and horizontal diffusivities with the sigma coordinate system. *Mon. Weather. Rev., 113,* 1380-1383, 1985.

Mellor, G. L., and T. Ezer, A Gulf Stream model and an altimetry assimilation scheme, *J. Geophys. Res., 96,* 8779-8795, 1991.

Mellor, G. L., and T. Yamada, Development of a turbulence closure model for geophysical fluid problems. *Rev. Geophys., 20,* 851-875, 1982.

Mellor, G. L., C. Mechoso, and E. Keto, A diagnostic calculation of the general circulation of the Atlantic Ocean, *Deep Sea Res., 29,* 1171-1192, 1982.

Mellor, G. L., T. Ezer, and L.-Y. Oey, The pressure gradient conundrum of sigma coordinate ocean models, *J. Atmos. Oceanic. Technol.,* in press, 1994.

Oberhuber, J. M., An atlas based on the COADS data set: The budgets of heat, uoyancy and turbulent kinetic energy at the surface of the global ocean, Rep. 15, *Max-Planck Inst. für Meteorol.,* Hamburg, Germany, 1988.

Oberhuber, J. M., Simulation of the Atlantic circulation with a coupled sea ice-mixed layer-isopycnal general circulation model, Model experiment, *J. Phys. Oceanogr., 23,* 830-845, 1993.

Oey, L.-Y., T. Ezer, G.L. Mellor, and P. Chen, A model study of 'bump' induced western boundary current variabilities, *J. Mar. Sys., 3,* 321-342, 1992.

Richardson, P. L., Average velocity and transport of the Gulf Stream near 55°W, *J. Mar. Res., 43,* 83-111, 1985.

Sarkisyan, A. S., and V. F. Ivanov, Joint effect of baroclinicity and bottom relief as an important factor in the dynamics of sea currents, *Izv. Acad. Sci. USSR Atmos. Oceanic Phys.,* Engl. Transl., *7,* 173-188, 1971.

Sarmiento, J. L., and K. Bryan, An ocean transport model for the North Atlantic, *J. Geophys. Res., 87,* 394-408, 1982.

Saunders, P. M., and S. R. Thompson, Transport, heat, and freshwater fluxes within a diagnostic numerical model (FRAN), *J. Phys. Oceanogr., 23,* 452-464, 1993.

Semtner, A. J., and R. M. Chervin, Ocean general circulation from a global eddy-resolving model, *J. Geophys. Res., 97,* 5493-5550, 1992.

Smagorinsky, J., S. Manabe, and J. L. Holloway, Numerical results from a nine-level general circulation model of the atmosphere, *Mon. Weather Rev., 93,* 727-768, 1965.

Sturges, W., Sea-surface topography near the Gulf Stream, Deep - Sea Res., *15,* 149-156, 1968.

Sturges, W., Sea level slope along continental boundaries, *J. Geophys. Res., 79,* 825-830, 1974.

Treguier, A. M., Kinetic energy analysis of an eddy resolving, primitive equation model of the North Atlantic, *J. Geophys. Res., 97,* 687-701, 1992.

Tziperman, E., and K. Bryan, Estimating global air-sea fluxes from surface properties and From climatological flux data using an oceanic general circulation model, *J. Geophys. Res., 98,* 22,629-22,644, 1993.

Tziperman, E., W. C. Thacker, R. B. Long, S.-M. Hwang, and S. R. Rintoul, Oceanic data analysis using a general circulation model, A North Atlantic model, *J. Phys. Oceanogr., 22,* 1458-1485, 1992.

Wunsch, C., The general circulation of the North Atlantic west of 50°W determined From inverse methods, *Rev. Geophys., 16,* 583-620, 1978.

T. Ezer and G. L. Mellor, Program in Atmospheric and Oceanic Sciences, P. O. Box CN710, Sayre Hall, Princeton University, Princeton, NJ 08544-0710. (e-mail: Internet ezer@splash.princeton.edu; glm@splash.princeton.edu)

(Received August 31, 1993; revised March 4, 1994; accepted March 21, 1994.)